Asian Journal of Convergence in Technology Volume IV Issue I
ISSN NO: 2350-1146 I.F-5.11

Microstructure Modeling and Neck Growth Analysis of Laser Sintered AlSi10Mg Nanoparticles

A Molecular Dynamics Study in Additive Manufacturing

Jyotirmoy Nandy, Seshadev Sahoo, Hrushikesh Sarangi
jyotirmoynanday@soauniversity.ac.in

Abstract*—*Molecular dynamics has been used in this work to study the sintering behavior and neck growth in laser sintered AlSi10Mg particles. The modeling is based on the experimental condition during which the laser power is varied and the scan speed is kept constant. The neck growth behavior is studied over two intervals of time. The results depict the increase in neck growth at higher heating conditions and also exhibits the accurate range of laser power that shall be used for achieving solid state sintering of AlSi10Mg.

Keywords*—*Additive Manufacturing; molecular dynamic; microstructure modeling.

I. INTRODUCTION

Direct metal laser sintering (DMLS) is a type of additive manufacturing process which consolidates powdered material with the help of high intensity laser power. The laser beam scans over the designed powder-spread area and binds the particles using the solidification reactions. Many previous works have reported the usage of macro sized particles [1] whereas in the recent times nano-sized particles are more into use [2]. Due to good casting properties and thin wall geometry, the usage of AlSi10Mg in DMLS has found its usage over a wide range of applications such as aerospace, manufacturing, tooling, prototyping and medical sectors. Various experimental studies have been found using AlSi10Mg in the DMLS process with respect to process parameters [3-5].

The physical and mechanical properties of the specimens produced by DMLS are of most importance. These properties are directly affected by the process parameters which are all used as inputs. However, early prediction of the microstructure evolution can be useful to save time as well as resources. These predictions can also be useful to select the appropriate range of parameters along with their suitable values. Using the wide range of modeling techniques, variations in microstructural changes can be easily analyzed and attempts can be made for further improvement. In the modern era, computational modeling has emerged to be the most powerful weapon for researchers all across the world. Using different time and length scales, computational modeling has allowed researchers to develop their insight and bring improvements. Incessant developments over the performance and accessibility of the computational tools have been carried out simultaneously to reduce the processing time and increase the efficiency.

Many attempts have been made in the past to model the sintering process using different alloys. Over the micro and macro scale, continuum modeling has been profoundly used to study the sintering behavior of the alloys [6-8]. However, these works can achieve validity only in conditions where the beam radius is comparatively greater than the particle radius. As a result, it is necessary to study the characteristic behavior of the alloys at the atomistic level. At a low energy input level, neck growth mechanisms and sintering rates have been analyzed using molecular dynamics (MD) for improving the commercial usage of elements such as gold and silver [9-11]. In a few more works, MD has also been used to study the mechanical properties of materials such as Ni-11/silica nanocomposites [12] and Cu nanoparticles [13]. Another study showcased the sintering behavior of Cu-Ag core shell structures such as nanoparticles and nanowires using the molecular dynamics at room temperature [14]. Few studies revealed the effect of temperature on coalescence of particles using selective laser sintering [15].

As it can be clearly observed from the literature, just a handful of atomistic modeling techniques have been put into use for examining the microstructure evolution of the DMLS process. Most of the works are carried out using selective laser sintering and selective laser melting process. Added to that, very less number of works include the use of ternary alloys. Most of the works have been based on analysis of binary alloys and composites. As combined to the field of DMLS, the usage of ternary alloys in modeling has not yet been carried out using atomistic approach. The usage of ternary alloys can prove to be promisingly efficient due to their profound user ability.

In this paper, MD approach has been used to study the solid-state sintering of laser sintered AlSi10Mg particles. A large scale atomistic model with laser sintered structures was developed where the particles are allowed to sinter. The temperature range was derived from the experimental conditions of DMLS. Neck width was calculated from the

results and was compared with time and temperature. A suitable range of temperature has been found after which the particles enter the stage of liquid state sintering.

II. SIMULATION DETAILS

All the MD simulations carried out in this work done using Large Scale Atomic/Molecular Massively Parallel Simulator (LAMMPS). A hybrid overlay pair styling has been used to model AlSi10Mg atoms. The classical Lennard-Jones (LJ) model has been used as a force field to describe the inter-atomic interactions between the two atoms of AlSi10Mg. The pairwise Lennard-Jones potential between two atoms at a distance of *r* from each other is described by [16] as follows:

$$U(r) = 4\varepsilon\left[\left(\frac{\sigma}{r}\right)^{12} - \left(\frac{\sigma}{r}\right)^{6}\right] \quad \ldots\ldots\ldots\ldots\ldots\ldots\ldots\ldots (1)$$

Where $\mathcal{E}$= depth of the potential well and σ = range of the potential. All measurements are expressed in units derived from the three basic units of energy $\mathcal{E}$, length σ and mass of an atom *m*. As an instance time unit t^* can be calculated as $t^* = \sigma(m/\varepsilon)^{1/2}$.

Three groups of atomistic models are developed as shown in Table 1. Their final temperatures are calculated using the thermal analysis. Every group consists of 2 particles with 32399 number of particles in each of them. Simulations using all three laser powers are carried out and the effect of temperature is studied in the sintering behaviour of AlSi10Mg. The scan speed is kept constant at 100mm/s.

TABLE 1: Simulations carried out in this study

Case	Laser Power (In Watts)	Temperature Range (In Kelvin)	State of Sintering
1.	70	300-754	Solid
2.	100	300-786	Solid
3.	130	300-850	Solid

III. STAGES OF SINTERING

The kinetics involved in sintering has been examined over the last few years. Experimental as well as theoretical aspects have shown interesting results over the process of sintering. However, distinguishing the stages the sintering has been a considerate point over these years and very few researchers have been able to provide the sufficient insights. Coble [16] was one of the very first to disintegrate the process of sintering into three different stages. According to his work, the first stage exhibits the neck formation and its evolution. The second stage corresponds to the development of particle openings where mainly the grain boundary diffusion takes place. The third and final stage of sintering takes place due to complete bulk diffusion. The particle openings dematerialize in the third stage as the inter-particle contact area reduces to its lowest. In the initial stage, the inter-particle area plays a vital role in the surface diffusion of the particles as the inter-contact area rises from 0 to 0.25 times of the cross-sectional area of the particles. This stage of sintering is commonly referred as the necking stage. In context to the inter-particle contact area, the second stage is marked by the discontinuity in the shape of the pores which further causes the evolution of the grain boundary diffusion. Also in the second stage, the grain boundary matrix comprising of the symmetrical dihedral angles has an enormous impact on the diffusion process overall. This occurs due to the location of the dihedral angles on the solid-vapor surface whose auxiliary locus is at the juncture along with the solid-solid surface. This juncture further comprises of the individual curved surfaces between the junctures. The last stage is a result of squeezing of the pore area. Figure 1 shows the stages of sintering.

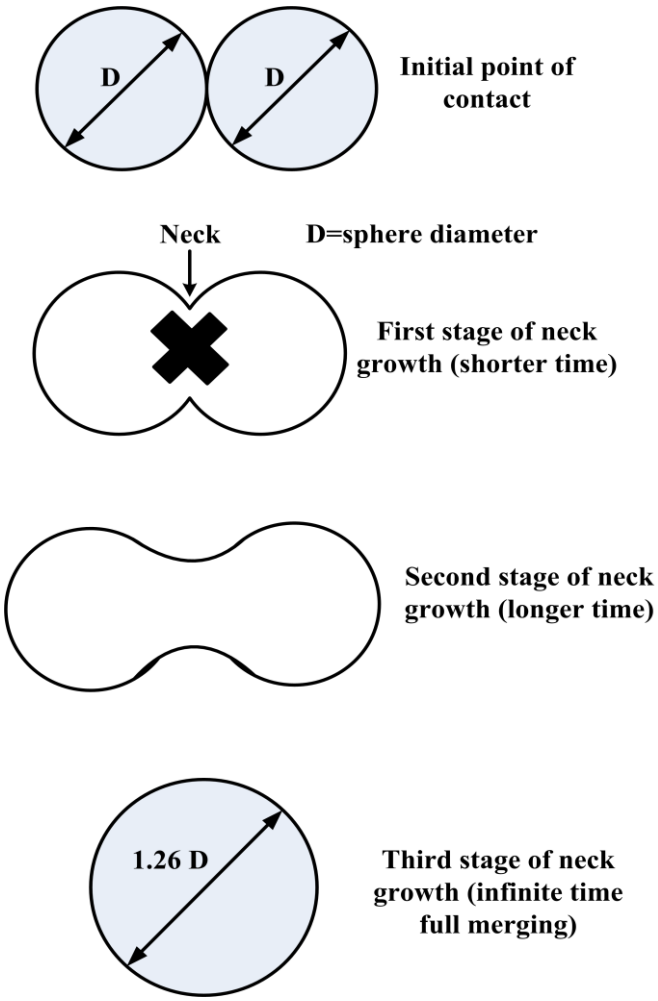

Fig. 1 Stages of sintering

A. Setting up an atomistic model

A two-particle pair setup is developed using a spherical AlSi10Mg clustered using the hybrid overlay pair style. Another replica is created and placed at a distance of 0.3nm with respect to the boundary to boundary distance. The AlSi10Mg-AlSi10Mg pair model is created using these two particles. The pair has a fcc lattice parameter. Every particle has a diameter of 4nm with 32299 number of atoms. The center to center distance between these two particles is maintained at 8.3nm. The nano-particle pair is shown in Fig. 2.

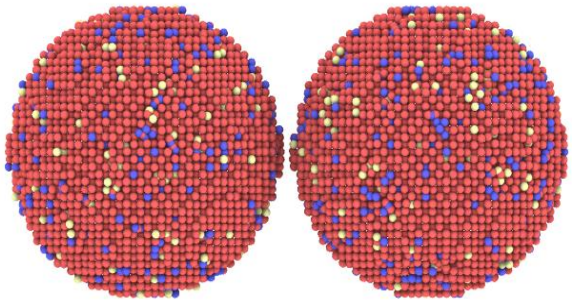

Fig. 2 Initial configuration of AlSi10Mg-AlSi10Mg pair model

B. Solid state sintering of AlSi10Mg-AlSi10Mg pair nanoparticles

A three-dimensional simulation box is created using the non-periodic shrink wrapped boundary condition in each direction. The neighboring criteria is maintained at the 'nsq' condition. The 'nsq' style of rendering the neighboring condition allows for a better scaling and also accelerates the simulation time. The randomization of all the atoms is carried out at 300K which is followed by the Maxwell-Boltzmann distributive aspect. To randomize the atoms in all directions, an initial temperature is maintained at 300K to fulfill the equilibration and relaxation condition. The time step is kept fixed at 0.001ps for the integration of equation of motion. Followed by the equilibration process, external heat is provided to the setup. The temperature range is maintained from 300K to 850K as derived from the thermal model in a time range of 50ps. The simulation is done at the system level. Dimensional variation is recorded and analyzed accordingly.

C. Neck growth calculation

The overall process of sintering can be evaluated using 4 stages according to the viscous flow model: the first point of contact, the preliminary stage of neck growth which occurs in the shorter interval of time, the intermediate stage of neck growth which takes place during the longer interval of time and the final stage where the two particles merge into each other. The last stage can be easily identified as the coalesced sphere acquires a diameter 1.26 times that of the starting one. However, in this study a time scale lesser than 20ps is attained to be the shorter interval. The longer interval of time is considered to be at a time scale above 20ps. Also, an important factor that has been considered while calculating the neck growth is that the time scale keeps reducing as the final temperature rises.

IV. Results and discussions

A. Solid state sintering of AlSi10Mg- AlSi10Mg nanoparticle pair

Temperature increase has been defined from 300K to 850K in 300000 time steps with each time step being 1.0^{e-15}s. The sintering profiles have been shown in the Fig. 3. It can be seen from the configuration changes occur during the 50ps time. The initial geometry of the particles boundaries has hardly made any contact with each other as shown earlier in Fig. 2. The energy minimization takes place as the temperature and time both increase. As a result, the migration of boundaries causes the movement of atoms near the boundaries. From Fig. 3(a), it can be well observed that the neck formation starts very early at only 5ps. By the time the atoms in the neck region start moving, the atoms on the surface start losing their crystal structure. The formation of the preliminary melt zone can be observed easily near the boundary area as shown in Fig. 3(b) and (c). By the time the simulation reaches 30ps the solid-state phenomena can be easily observed as that shown in Figure 3(d).

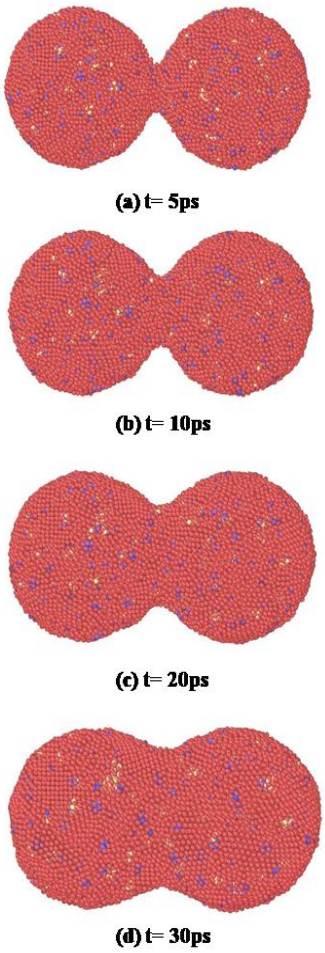

Fig. 3 MD sintering profiles of AlSi10Mg in solid state sintering conditions at different timesteps (a)5ps (b)10ps (c)20ps (d)30ps

B. Neck growth behavior of AlSi10Mg- AlSi10Mg nanoparticle pair

The short time interval of sintering in this study has been maintained at 20ps. After this time limit, the longer time interval is attained. The neck growth behavior of AlSi10Mg-AlSi10Mg nanoparticle pair has been studied under the NVT ensemble. In this canonical ensemble, the time integration is done over the Noose-Hoover style non-Hamiltonian equations of motion. The position and velocities of atoms are updated in every timestep. The laser power and temperature range mentioned in Table 1 are used to perform this simulation and study the necking formation. The variation of neck growth with respect to different laser powers are calculated. Figure 4 shows the neck formation at different laser powers for the shorter interval of time, i.e. till 20ps.

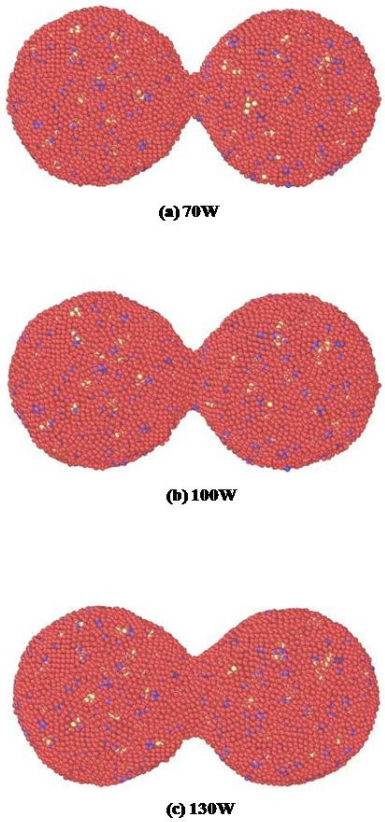

Fig. 4 MD sintering profiles of AlSi10Mg in short interval of time (20ps) at different laser powers (a)70W (b)100W (c)130W

From Fig. 4 it can be seen clearly that the configuration changes occur due to the increase in laser power. At 70W power, the necking has starts in the range of 10-15ps as shown in Fig. 4(a). With the increase in laser power, the neck width increases between the particles. At 100W and 130W, neck width is comparatively larger as compared to that in 70W. From Fig. 4(b) and 4(c), it can be observed that the higher temperature causes the diffusion process to accelerate enormously as the inter-contact area rises from 0-0.25 times that of particle size. Also, with the increase in temperature the grain boundary energy reduces in a faster rate.

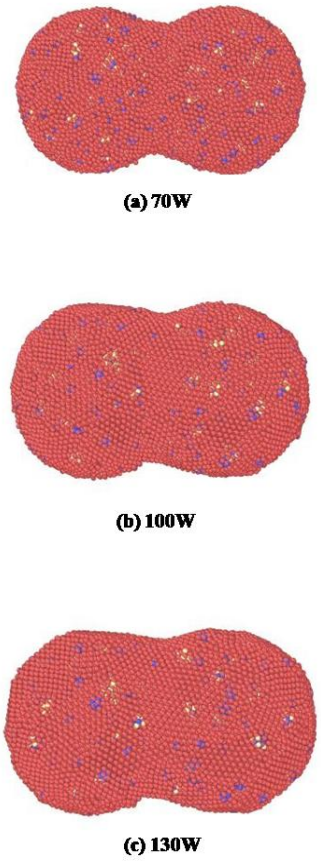

Fig. 5 MD sintering profiles of AlSi10Mg in long interval of time (above 20ps) at different laser powers (a)70W (b)100W (c)130W

Figure 5 shows the neck growth behavior of AlSi10Mg-AlSi10Mg pair in the long interval of time. After 20ps, the surface diffusion starts which causes the inter-particle area to reduce more efficiently. With the increase in temperature the necking increases rapidly in Fig. 5(a) and (b). One noticeable outcome through the simulation result can be derived from Fig. 5(c). Very less change in the neck growth can be observed as compared to Fig. 5(b). This is caused due to the loss of inter-particle area at 130W. Due to the reduction in pore area, the curved surfaces show less movement due to partial diffusion. Also, volumetric bulk diffusion starts after this range where the sintering tends to enter the liquid state.

Another easier technique that can be used to study the neck growth is by measuring the dimensional change in the particles. Using geometrical relation the neck width can be evaluated using the particle diameter d_1 and total length d_2 as shown in Fig. 6. It shows the total reduction in length with increase in temperature and time. The atoms near the boundary start moving towards the atoms near the neck region. Also it can be observed that there is very less change

in the diameter of particles. Figure 7 shows the neck growth behavior with respect to power. It can be seen that the neck width increases with increase in laser power.

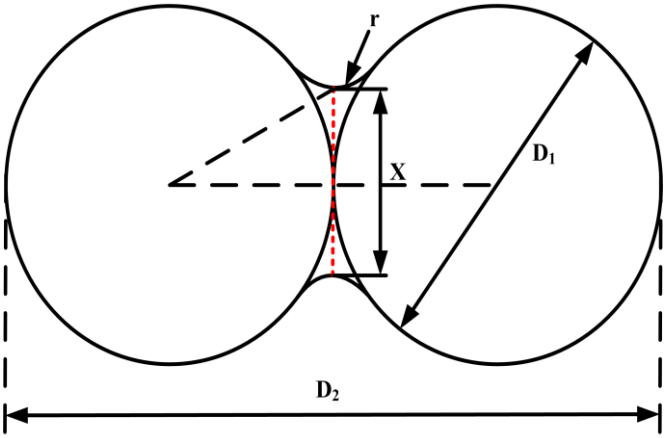

Fig. 6 Dimensions in a two particle sintering model [17]

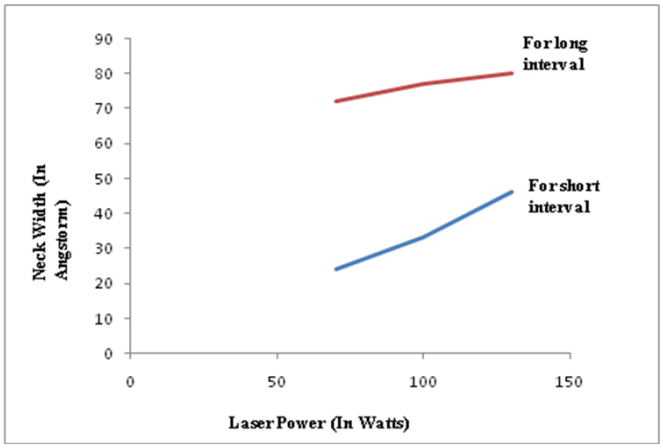

Fig. 7 Neck growth Vs laser power

V. Conclusion

MD simulations were carried out using the hybrid overlay technique for AlSi10Mg-AlSi10Mg nanoparticle pair. At different laser powers, the temperature ranges are extracted and applied in this simulation. The results show that the increase in laser power causes faster neck growth formation in both short and long time intervals. The increase in neck width was found to be proportional to laser power. Also, the suitable range for laser power input was found to be at 130W for solid state sintering.

References

[1] D. Manfredi, R. Canali, M. Krishnan, E. P. Ambrosio, F. Calignano, M Pavese, L Miranti, S. Belardinelli, S. Biamino and P. Fino, "Aluminium matrix composites (AMCs) by DMLS." High Value Manufacturing: Advanced Research in Virtual and Rapid Prototyping: Proceedings of the 6th International Conference on Advanced Research in Virtual and Rapid Prototyping, Leiria, Portugal, 1-5 October, 2013. Vol. 195. No. 180,195. CRC Press, 2013.

[2] M. Lorusso, A. Aversa, D. Manfredi, F. Calignano, E. Ambrosio, D. Ugues and M. Pavese, "Tribological Behavior of Aluminum Alloy AlSi10Mg-TiB2 Composites Produced by Direct Metal Laser Sintering (DMLS)", J Mater. Eng. Perform., vol. 25, no. 8, pp. 3152-3160, 2016.

[3] M. Krishnan, E. Atzeni, R. Canali, F. Calignano, D. Manfredi, E. P. Ambrosio and L. Iuliano, "On the effect of process parameters on properties of AlSi10Mg parts produced by DMLS." Rapid Prototyping J, 20.6, 449-458, 2014.

[4] B.A. Fulcher, D.K. Leigh, and J.W. Trevor, "Comparison of AlSi10Mg and Al 6061 processed through DMLS." Proc. of the Solid Freeform Fabrication (SFF) Symposium, Austin, TX, USA. Vol. 46. 2014.

[5] E. Atzeni and S. Alessandro, "Study on unsupported overhangs of AlSi10Mg parts processed by Direct Metal Laser Sintering (DMLS)." Journal of Manufacturing Processes 20 2015: 500-506.

[6] F. Niebling, A. Otto and M. Geiger, "Analyzing the DMLS-process by a macroscopic FE-model." Proc. of 13th Solid Freeform Fabrication Symposium. 2002.

[7] N. N'Dri, H.W. Mindt, B. Shula, M. Megahed, A. Peralta, P. Kantzos and J. Neumann, "DMLS Process Modelling and Validation." TMS 2015 144th Annual Meeting & Exhibition. Springer, Cham, 2015.

[8] J. Nandy, H. Sarangi and S. Sahoo, "Modeling of microstructure evolution in direct metal laser sintering: A phase field approach." IOP Conference Series: Materials Science and Engineering. Vol. 178. No. 1. IOP Publishing, 2017.

[9] H. Pan, H. Seung, H. Ko and P. C. Grigoropoulos. "The solid-state neck growth mechanisms in low energy laser sintering of gold nanoparticles: a molecular dynamics simulation study." J Heat Trans, 130.9 (2008): 092404.

[10] S. Jiang, Z. Yuwen, G. Yong, C. Zhen and P. Hao, "Molecular dynamics study of neck growth in laser sintering of hollow silver nanoparticles with different heating rates." J Phys D: Applied Physics 46.33 (2013): 335302.

[11] L. Yang, G. Yong, Z. Yuwen and JK Chen, "Molecular dynamics simulation of neck growth in laser sintering of different-sized gold nanoparticles under different heating rates." Appl Phys A 106.3 (2012): 725-735.

[12] H. Chun and S. Das, "Functionally graded Nylon-11/silica nanocomposites produced by selective laser sintering", Mater Sc Eng: A. 2008 Jul 25;487(1):251-7.

[13] S. Yang, K Wonbae and C. Maenghyo, "Molecular dynamics study on the coalescence kinetics and mechanical behavior of nanoporous structure formed by thermal sintering of Cu nanoparticles." Int J Eng Sc 123 (2018): 1-19.

[14] J. Wang and S. Seungha, "Room temperature molecular dynamics simulations on the sintering of Cu-Ag core shell structures: Nanoparticles and nanowires", (2016).

[15] S. L. Cheung, C. K. Chua, K. Zhou and J. Wei, "Effects of Temperature on Particle Coalescence in the Selective Laser Sintering Process," (2014).

[16] R. L. Coble, "Sintering crystalline solids. I. Intermediate and final state diffusion models." J Appl. Phys. 32.5 (1961): 787-792.

[17] A. Moitra, S. Kim, S. G. Kim, S. J. Park, R. M. German, R.M. and M. F. Horstemeyer, "Investigation on sintering mechanism of nanoscale tungsten powder based on atomistic simulation." Acta Materialia, 58.11 (2010): 3939-3951